A&A 420, 233–243 (2004)
DOI: 10.1051/0004-6361:20040091

Astronomy & Astrophysics

IR spectroscopic study of olivine, enstatite and diopside irradiated with low energy H^+ and He^+ ions

K. Demyk[1], L. d'Hendecourt[2], H. Leroux[3], A. P. Jones[2], and J. Borg[2]

[1] PhLAM, Université des Sciences et Technologies de Lille, 59655 Villeneuve d'Ascq Cedex, France
[2] IAS-CNRS, "Astrochimie Expérimentale", Université Paris XI, Bâtiment 121, 91405 Orsay Cedex, France
[3] LSPES, ESA CNRS 8008, Université Sciences et Technologies de Lille, 59655 Villeneuve d'Ascq Cedex, France

Received 28 July 2003 / Accepted 27 February 2004

Abstract. In this article we investigate the interaction of silicate grains with light atoms ionized and accelerated during the propagation of shock waves in the diffuse interstellar medium (ISM). Such an interaction which is equivalent to the irradiation of the grains with accelerated ions, is a potentially important process for silicate grain evolution in the ISM. We present the results of irradiation experiments aimed at simulating this process. The same crystalline silicates as those identified around evolved stars before their injection in the ISM, forsterite, enstatite and diopside, were irradiated with light ions (H^+, He^+) at low energies (10–50 keV). The IR spectroscopic characteristics of the samples were analyzed before and after the irradiation in the 2–35 μm range allowing us to study the structural modifications in the irradiated minerals. The experiments show that low energy H^+ (10 keV) and He^+ ($\leq$50 keV) ions efficiently amorphize crystalline silicates with fluence $\leq 10^{18}$ ions/cm^2. Since these experimental conditions are compatible with interstellar environments, the interaction of grains with high velocity shock waves may be responsible for the absence of crystalline silicates in the ISM. The comparison of the IR spectra of the irradiated silicates with observations of the Galactic Center is presented. This comparison calls into question the classical assignment of the interstellar amorphous silicate bands.

Key words. methods: laboratory – ISM: dust, extinction – ISM: evolution – shock waves

1. Introduction

The diversity of composition and structure of silicate dust was revealed by the spectroscopic data from the Infrared Space Observatory, ISO (de Graauw et al. 1996). From the interpretation of infrared (IR) spectra of different environments such as young and evolved stars, interstellar clouds, protostars, comets..., it has become clear that the nature of the silicate dust varies with the environment. In particular a component of crystalline silicates was discovered in the IR spectra of some evolved stars, the birth site of the silicate dust, around planetary nebulae and around some young stars (e.g. Waters et al. 1996; Waelkens et al. 1996). The spectral signature of this crystalline dust consists of sharp bands observed in most ISO spectra at wavelengths greater than $\sim$20 μm, usually in emission and in a few cases in absorption (e.g. Sylvester et al. 1999). These bands are due to the vibration of the crystalline lattice of the grains. Because they are very specific to the composition and to the atomic arrangement, it is possible to determine the carriers of the observed bands, mostly enstatite, forsterite and diopside (e.g. Demyk et al. 2000; Kemper et al. 2002). Although the crystalline silicate component may represent up to 20% of the total mass of the silicate in the objects where they are observed, none of these bands has been observed in the IR spectra of the interstellar medium (ISM) (Lutz et al. 1996; Schutte et al. 1998) in which the silicate dust appears to be completely amorphous. This is also the case in the spectra of class 0 protostars (Demyk et al. 1999). The abundance of crystalline silicates that may be present in the ISM, not being detectable in the IR spectra, has been estimated by Li & Draine (2001) to be at most 5%.

Evolved stars, planetary nebulae, interstellar clouds, protostars, young stars and comets constitute different stages of the life cycle of the dust. During its life cycle the silicate dust, in permanent interaction with its surrounding, is submitted to different physical processes susceptible to alter its structural and chemical properties. Among them the interaction of grains with accelerated ions may play an important role in explaining the transformation of the silicates from their birth site around evolved stars to the ISM. In the last 20 years, several experimental studies of silicate irradiation have been performed with experimental conditions more or less compatible with the astrophysical case. For example the interaction between olivine grains and H^+ and He^+ ions accelerated at energies of 4–20 keV in the solar wind, was proven to be an efficient mechanism for explaining the amorphous rim observed around the lunar regolith grains and around Interplanetary Dust Particles (IDPs)

Send offprint requests to: K. Demyk,
e-mail: karine.demyk@univ-lille1.fr

(Borg et al. 1979; Borg 1982; Bradley 1994); in contrast to high energy (≥1 MeV) protons which do not induce structural changes in olivine micron grains (Day 1977). In a previous paper we reported the first experimental study aimed at explaining the absence of crystalline silicates in the ISM as a consequence of their interaction with low energy ions accelerated in supernova shock wave propagation (Demyk et al. 2001). We showed that the irradiation of olivine with 4–10 keV He^+ ions destroys the crystalline structure of the olivine and amorphizes it completely. Changes in the composition of the irradiated sample were analyzed in detail (Carrez et al. 2002) and this study reveals that the olivine loses oxygen and magnesium during the irradiation. Recently Jäger et al. (2003) performed irradiation experiments on enstatite with He^+ and Ar^+ ions in the 50–400 keV energy range.

In this article we continue our experimental study started in the papers by Demyk et al. (2001) and Carrez et al. (2002). In addition to olivine we have also studied the irradiation of enstatite and diopside, the two others crystalline species that have been identified around evolved stars. We have used He^+ ions and also H^+ ions with low energies (10–50 keV). The studied samples were analyzed by IR spectroscopy in the 2–35 μm range. Although IR spectroscopy is not very sensitive to chemical changes in the samples it is extremely sensitive to structural changes. Furthermore it allows us to compare the experimental results with astronomical observations. The experiments and analysis of the irradiated samples are described in Sect. 2. The results, presented in Sect. 3, are discussed in Sect. 4. The astrophysical implications are presented in Sect. 5.

2. Experiments

The samples studied in these experiments are the San Carlos olivine ($Mg_{1.8}Fe_{0.2}SiO_4$), enstatite ($Mg_{1.85}2Fe_{0.1}Ca_{0.05}Si_2O_6$) and diopside ($Ca_1Mg_{0.85}Fe_{0.15}Al_{0.1}Si_{1.95}O_6$). The compositions are deduced from microanalysis performed with a transmission electron microscope equipped with an X-ray Energy Dispersive Spectroscopy system. The samples were irradiated with the ion source SIDONIE at the CSNSM (Centre de Spectrométrie Nucléaire et de Spectrométrie de Masse, Orsay, France) and then analyzed by IR transmission microspectroscopy at LURE (Laboratoire pour l'Utilisation du Rayonnement Électromagnétique, Orsay, France) and at the BNL (Brookhaven National Laboratory, Brookhaven, USA). We used He^+ and H^+ ions at energies of 10, 20 and 50 keV with fluences of 10^{18} ions/cm^2 (see Table 1). The irradiation was performed at room temperature and the current density was kept low-enough (≤9 μA) so as to prevent sample heating.

The samples were prepared in such a way that the volume analyzed with IR spectroscopy is fully irradiated. This was chosen to avoid the superposition of non-irradiated, crystalline sample, which exhibits strong and sharp spectral features at the same wavelengths as the irradiated, fully or partly amorphized, sample. The penetration depth of H^+ and He^+ ions at energies of 10, 20 and 50 keV is of the order of 100–400 nm (Fig. 1). Since the IR measurements are performed in transmission, the constraint that the volume analyzed with the IR beam is fully irradiated limits the maximum thickness of the samples to the penetration depth of the ions. Such small thicknesses can be obtained using the sample preparation used for the study of IDPs, i.e. by using ultra-microtome sections of the samples. The samples were ground in an agate mortar down to submicron size. A small amount of this powder was incorporated into epoxy. Then microtome sections of the desired thickness were made and deposited on carbon coated grids suitable for an analysis of the samples by transmission electron microscopy (TEM). These minerals are hard and thus difficult to cut, and thus only grains smaller than 1 μm were used. The size separation was performed by sedimentation in alcohol. For the same reason, the thickness of the sections was limited to 200 nm. Several sections are deposited on one TEM grid. Each section contains numerous mineral grains. The sample geometry is shown in Fig. 2. Figure 3 presents TEM bright field images of a non-irradiated microtome section of olivine and of microtome sections of enstatite, diopside and olivine after irradiation.

Because the volume of material fully irradiated is very small, conventional FTIR spectroscopy is not sensitive-enough. We therefore performed the experiments using an IR microscope coupled to a FTIR spectrometer and a synchrotron radiation source. This technique allows us to study micron-size areas of the samples and to thus get a good spectral contrast. It also

Table 1. The studied samples.

Sample name	Mineral	Thickness	Ions	Energy
E0	Enstatite	200 nm	–	–
E1	Enstatite	200 nm	He^+	20 keV
E2	Enstatite	200 nm	He^+	50 keV
O0	Olivine	100 nm	–	–
O1	Olivine	70 nm	He^+	20keV
O2	Olivine	200 nm	He^+	50keV
D1	Diopside	90 nm	He^+	20 keV
D2	Diopside	140 nm	H^+	10 keV

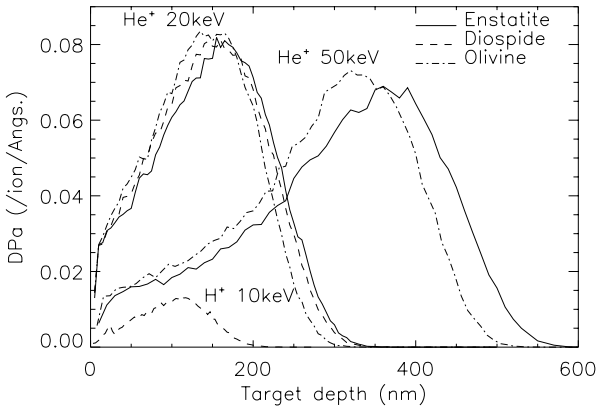

Fig. 1. The number of displaced atoms per ion/Å in olivine, diopside and enstatite for 10 keV H^+ and 20 and 50 keV He^+ incident ions. The maximum of the curves represents the penetration depth of the incident ions into the mineral. The simulations were performed using the program TRIM (TRansport of Ions in Matter, Ziegler et al. 1996).

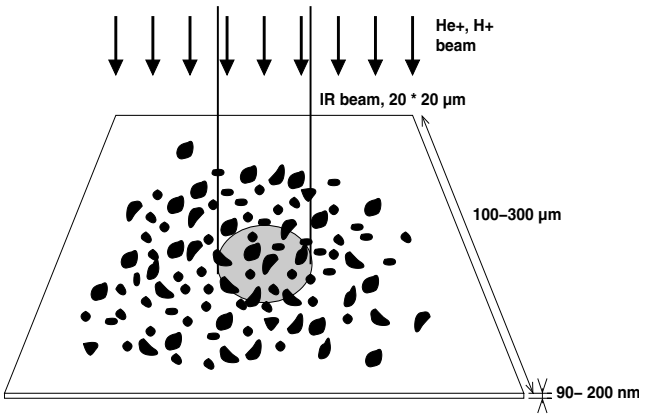

Fig. 2. Experimental configuration for sample irradiation and analysis. See text Sect. 2.

allows us to improve the signal to noise ratio because of the use of a bright source, the synchrotron radiation. Preliminary studies were made in the 2–15 μm range with the IR microspectrometer (NIcolet NicPlan) in line with the synchrotron radiation in LURE (Orsay, France), with a KBr beamsplitter and a nitrogen-cooled MCT detector. A similar instrument, with a broader spectral coverage, is also in line at the synchrotron radiation source at the NSL (Brookhaven, NY, USA). We obtain the IR spectra of our samples in the 5–30 μm range (Si beamsplitter and a nitrogen-cooled MCT detector) and in the 13–50 μm range (same beamsplitter, He-cooled CoGe detector). In both cases the size of the IR spot on the sample is diffraction-limited and was set to $\sim 20 \times 20$ μm. As shown in Fig. 2 the IR beam thus averages on several grains on a microtome section.

3. Results

3.1. Enstatite

Figure 4 presents the IR spectra of the non-irradiated enstatite microtome grid E0 measured at the NSL with two configurations allowing us to cover the 2–50 μm spectral range. Both spectra overlap well and the long wavelength spectrum allows us to better resolve the contrast of the bands at $\lambda \geq 30$ μm. The microscope spectra compare well with the spectrum of submicron enstatite grains embedded in CsI, measured with a classic FTIR spectrometer (Bruker IFS66V) at the IAS (Orsay, France), except for two bands at 8.0 and 8.45 μm which are due to absorption from the epoxy in which the grains are embedded. The good comparison between the spectra shows that the geometry of the samples does not affect their IR signature. The spectra of all the irradiated grids were measured at LURE in the 2–16 μm range before irradiation. In the overlapping spectral region, all the spectra are in very good agreement with the spectrum of the sample E0 measured at Brookhaven and with the spectrum of the enstatite in a CsI pellet.

The spectra of the grids E1 and E2, measured after irradiation with 20 keV and 50 keV He^+, respectively, are compared with the spectrum of the non-irradiated grid E0 in Figs. 5 and 6. For each grid several zones, corresponding to different areas on the same microtome section or to different microtome sections on the grid, were analyzed. A rapid look at the data reveals dramatic changes in the IR spectral signature of the irradiated samples compared to the non-irradiated sample E0. Theses changes illustrate the structural alteration of the crystalline enstatite resuting from the effect of irradiation. The numerous sub-peaks in the stretching and bending modes of the crystalline sample are more or less completely absent in the spectra of the irradiated samples, depending on the analyzed zone. These spectra present two broad and structure-less bands characteristic of amorphous silicate materials, indicating that the enstatite is fully or partly amorphized by the He^+ irradiation depending on the area chosen for the analysis. The irradiation also alters the epoxy in which the grains are embedded. Consequently the two bands due to the epoxy at 8.0 and 8.45 μm are absent in the spectra of the irradiated samples. This is also true for the irradiated olivine and diopside samples (see below).

A closer look at Fig. 5 shows that the spectra of the irradiated samples present some differences. The stretching mode is at 9.85 μm in all spectra. However, the shape of the band varies from one zone to another because some structure remains in the band after the irradiation. The presence of structure in the stretching mode results in an increase of the *FWHM* (Full Width at Half Maximum) of the band. The spectra E2a and E1a which are the most structureless have a *FWHM* of 2.35 μm whereas the spectrum of E2b which shows more structure in the stretching mode has a *FWHM* of 2.60 μm. In all cases, the bending mode appears to be completely structureless. It peaks in the 18.8–19.8 μm range. The uncertainty on the peak position is related to the continuum division which also affects the shape of the bending mode, especially its red wing. Indeed, because the 5–30 μm spectral range ends in the red wing of the bending mode it is in some cases difficult to estimate the level of the continuum at $\sim$25–30 μm. This also prevents us from getting a reliable estimate of the ratio of the stretching to the bending bands. The two spectra taken in the 13–50 μm region, for which no continuum have been subtracted, thus appear to be the most reliable to determine the bending mode position and its shape but not the $\tau_{\text{stret.}}/\tau_{\text{bend.}}$ ratio since the stretching mode is not observed in this spectral range. In these two spectra the bending mode peaks at 19.3 μm.

3.2. Diopside

The diopside samples were irradiated with He^+ at 20 keV and H^+ ions at 10 keV. The IR spectra of the irradiated diopside are shown Figs. 7 and 8. Since prior to irradiation the IR spectra of the diopside grids were only measured up to 15 μm at LURE, we use the spectrum of submicron grains embedded in CsI for comparison. In the overlapping spectral range the microscope spectra of the non-irradiated grids compare well with the spectrum of the diopside pellet.

As for the case of enstatite, the changes in the spectral signature of the samples are notable. The bands characteristic of the crystalline structure completely disappear in some areas of the D1 grid (D1a). Some structure remains in the other spectra. This again indicates that diopside is amorphized by ion

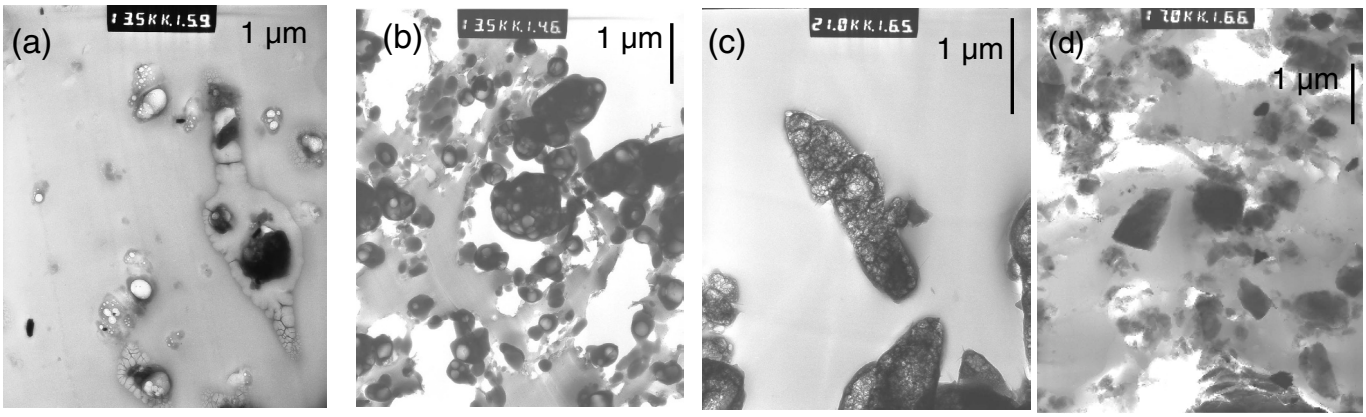

Fig. 3. TEM bright field images of ultra-microtome sections of **a)** enstatite, **b)** diopside and **c)** olivine grains after irradiation, and **d)** non-irradiated olivine grains. The epoxy in which the grains are embedded and the carbonaceous film of the TEM grid on which the sections are deposited constitute the gray background surrounding the grains. As can be seen in **a)** and **b)** the epoxy and the carbonaceous film are damaged by irradiation. Note that the grains are rounded by the irradiation and contain bubbles of implanted ions, this is clearly not the case for the non-irradiated sample shown in **d)**.

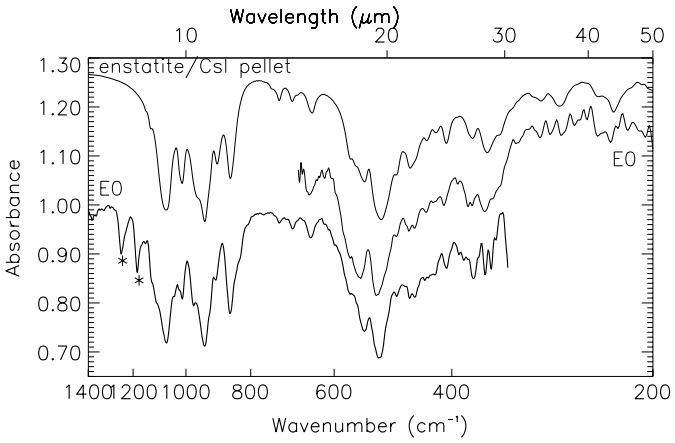

Fig. 4. IR spectra of the microtome section E0 of the non-irradiated enstatite measured with the IR microscope (two lower curves) compared to the spectrum of submicron enstatite grains embedded in a CsI pellet (upper curve). The bands labelled with stars are due to absorption by the epoxy in which the grains are embedded. All spectra were divided by a continuum (except the FIR spectrum) and were normalized to the bending mode at ~20 μm. The spectra have been shifted for clarity.

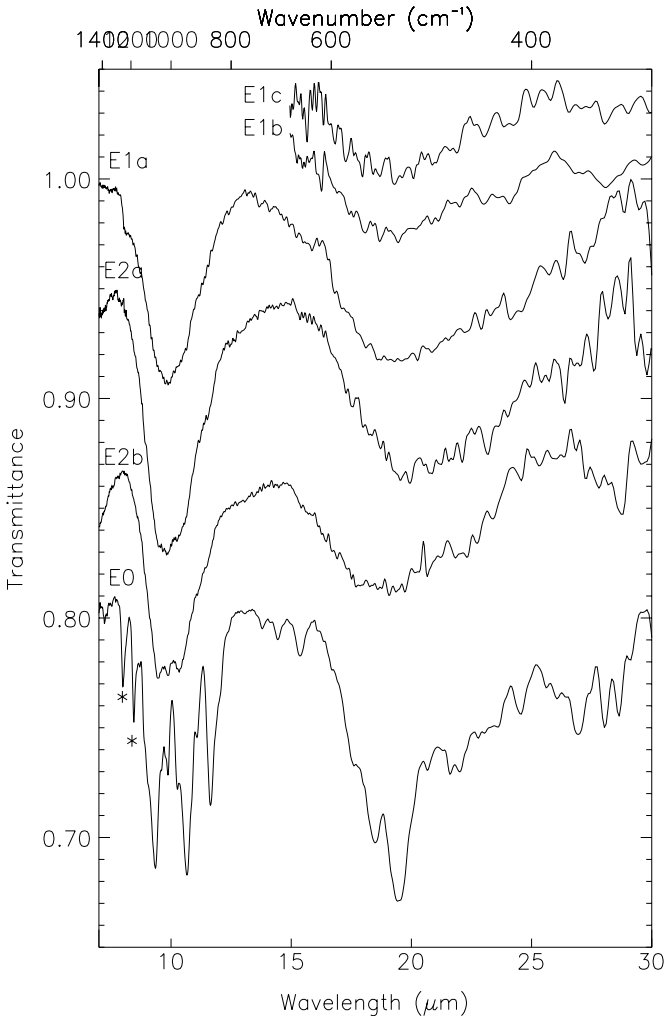

Fig. 5. IR spectra of the microtome sections of enstatite measured after irradiation compared to the spectrum of the non irradiated grid E0 (bottom trace). The bands labelled with stars are due to absorption by epoxy in which the grains are embedded. All spectra were divided by a continuum and shifted for clarity.

irradiation, fully amorphized for the 20 keV He^+ irradiation and almost completely for the 10 keV H^+ irradiation.

The position of the stretching mode in the fully amorphous spectrum D1a is 10.0 μm its *FWHM* is 2.3 μm. The spectra are of better quality than those for enstatite, thus the precision on the peak position and on the shape of the bending mode is better. The bending mode is structureless in three spectra (D1a, D1b and D2a) and its position is, respectively, 20.5, 20.6, 20.45 μm.

The remaining structure in the spectra D2a,b,c and D1a indicates that the grains are only partly amorphized and that some crystalline material is still present. The spectral changes from the D2c spectrum to the D1a spectrum may be viewed as the evolution of the spectroscopic characteristics as more and more material is amorphized during the irradiation. As in the case of

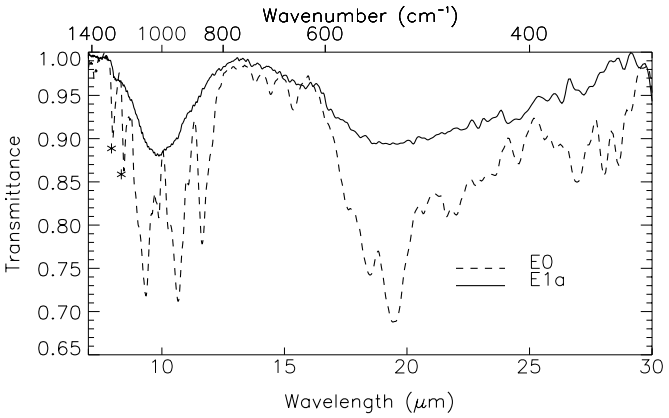

Fig. 6. IR spectra of the microtome section E0 of the non-irradiated enstatite measured with the IR microscope (dashed line) compared to the spectrum of the microtome section of enstatite measured after irradiation (continuous line). The bands labelled at 8.0 and 8.45 μm are due to absorption by epoxy in which the grains are embedded.

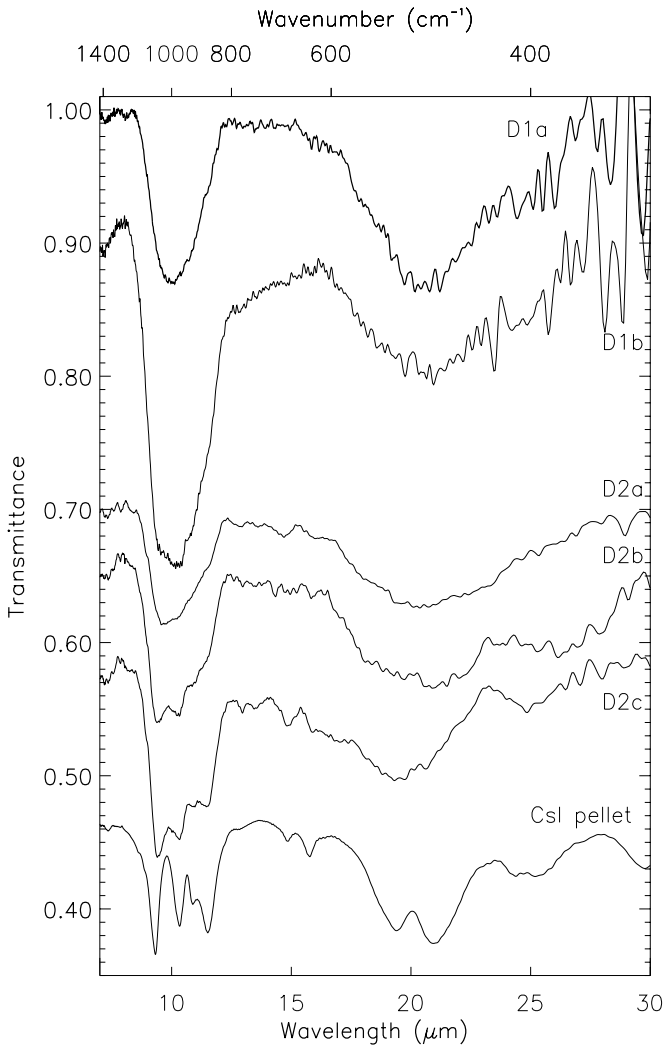

Fig. 7. IR spectra of the microtome sections of diopside measured after irradiation compared to the spectrum of a CsI pellet containing submicron grains of diopside (lower curve). The spectra were divided by a continuum and shifted for clarity.

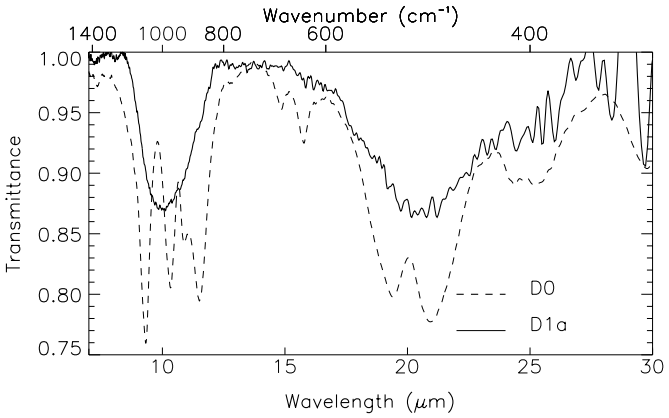

Fig. 8. IR spectra of diopside in a CsI pellet (dashed lines) compared to the spectrum of the microtome slice of diopside measured after irradiation (continuous line).

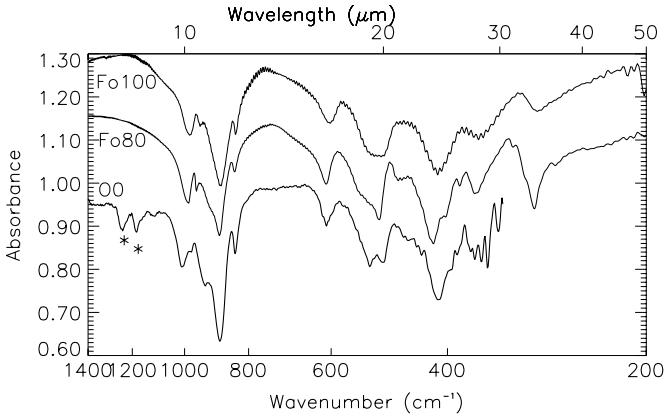

Fig. 9. IR spectra of the microtome section O0 of the non-irradiated olivine measured with the IR microscope (lower curve) compared to the spectra of submicron olivine grains embedded in a CsI pellet (upper curve). The olivine used for the measurements are synthetic forsterite (Fo100, upper curve) and olivine containing 20% fayalite (Fo80, middle curve). Both samples were obtained courtesy of C. Koike. The bands labelled with stars are caused by absorption by the epoxy in which the grains are embedded. All spectra were divided by a continuum and were normalized to the bending mode at ~20 μm. The spectra have been shifted for clarity.

enstatite, we note that the bending mode bands and the bands at longer wavelengths are the first to disappear during irradiation.

3.3. Olivine

The spectrum of the non-irradiated olivine grid O0 is presented Fig. 9. For comparison the spectra of submicron synthetic olivine grains embedded in CsI are shown. The two spectra correspond to pure forsterite and to olivine containing 20% of fayalite. The natural sample used in these experiments contains ~10% of fayalite. The spectral agreement is very good. This is also the case for all the microscope spectra of the grids O1 and O2 measured at LURE before the irradiation.

Figures 10–12 present the spectra of the O1 and O2 grids measured after the irradiation at LURE and at Brookhaven. The spectra measured at LURE are characteristic of a fully

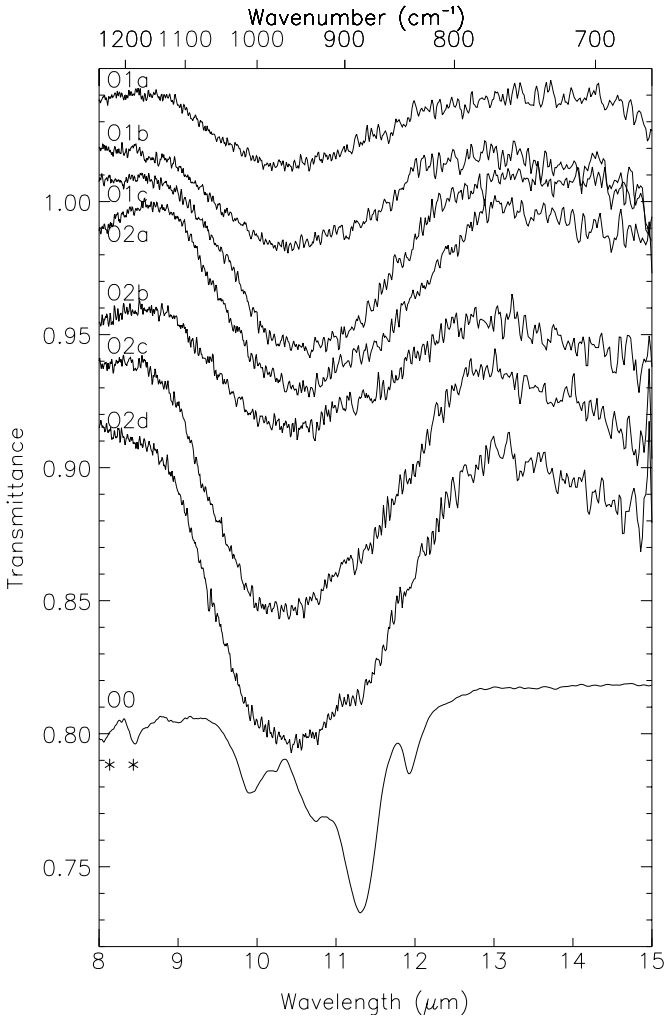

Fig. 10. IR spectra of the microtome sections of olivine measured at LURE after irradiation compared to the spectrum of the non-irradiated grid O0 measured at Brookhaven (lower curve). The bands labelled with stars are caused by absorption from the epoxy in which the grains are embedded. All spectra were divided by a continuum and shifted for clarity.

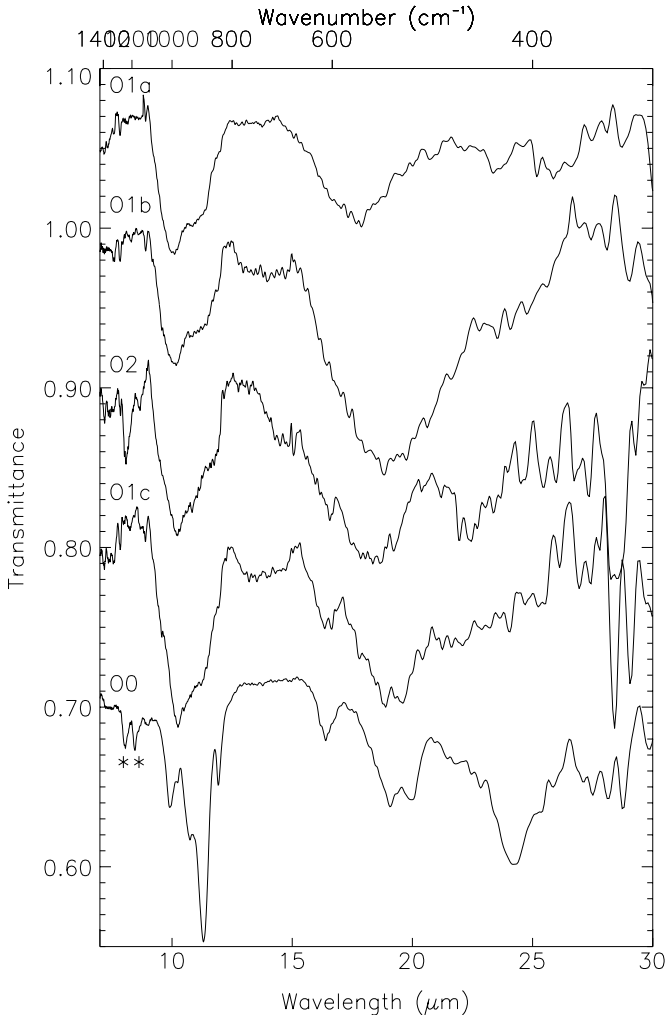

Fig. 11. IR spectra of the microtome sections of olivine measured after irradiation compared to the spectrum of the non-irradiated grid O0 (lower curve). The bands labelled with stars are caused by absorption by the epoxy in which the grains are embedded. All spectra were divided by a continuum and shifted for clarity.

amorphized material (Figs. 10 and 12). No structure remains in the stretching mode except a weak shoulder at 11.3 μm in the O2d spectrum. The position of the stretching mode is ~10.3–10.6 μm and its *FWHM* is ~2.3–2.4 μm. The uncertainty in this value probably comes from the continuum determination which is difficult to estimate at long wavelengths as we have no information on the bending mode. Unfortunately, at Brookhaven, the grids appeared damaged and we were not able to find the completely amorphous areas (Fig. 11). Consequently, some of the bands characteristic of the crystalline samples are still visible in the spectra. Another consequence of the poor quality of the grid is the difficulty in getting good spectra, especially beyond 20–25 μm. Thus, as in the case of enstatite, the determination of the continuum is sometime difficult as illustrated by the comparison of the O1a and O1b (Fig. 11) spectra in which the bending mode peaks at 17.85 μm and 18.87 μm, respectively. In these spectra the crystalline band at 24.2 μm is present as a shoulder in the red wing of the

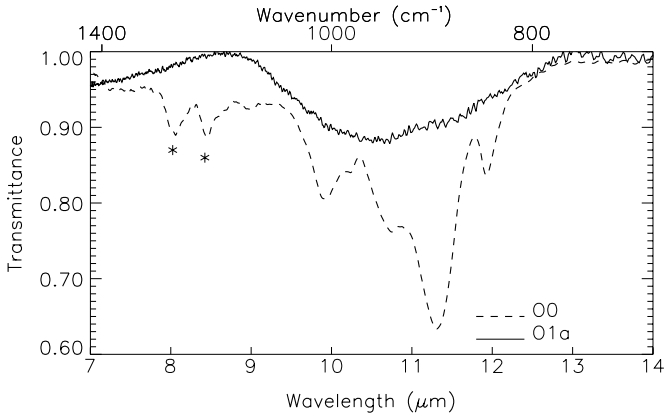

Fig. 12. IR spectra of the microtome section O0 of the non-irradiated olivine with the IR microscope (dashed line) compared to the spectrum of the microtome slice of olivine measured after irradiation (continuous line). The bands labelled at 8.0 and 8.45 μm are caused by absorption by the epoxy in which the grains are embedded.

bending mode. The crystalline bands are more prominent in the spectra of O1c and O2.

4. Discussion

As expected, irradiation with low energy light ions (10–50 keV H^+ and He^+) induces a strong modification of the IR spectral signature of silicates. The most important effect is the progressive disappearance of the features characteristic of the initial crystalline material. We note that the long wavelength bands are the first ones to disappear from the spectra. This is particularly well illustrated in the case of enstatite for which the bending mode is structureless for all spectra even for those which show structure in the stretching mode (Fig. 5). The long wavelength crystalline bands involve the vibration of the crystalline lattice (at $\lambda \geq 20$–25 μm), and the bending modes of O-Si-O bonds and other 3-atom bond groupings. As soon as irradiation starts the crystalline lattice is damaged and its characteristic vibrations vanish. Similarly, the breaking of bonds induced by the irradiation primarily affects the bending vibrations which involve 3 atoms. Thus these modes disappear first whereas the stretching vibration modes, less affected by the irradiation, may persist in the IR spectra.

From Figs. 5, 7, 11 it can be seen that in some cases the stretching and bending modes in the spectra of various zones on the same grids show different degrees of structure (see for example spectra E2a and E2b in Fig. 5, spectra D2a,b,c in Fig. 7, and spectra O1a,b,c in Fig. 11). Theses spectral differences may be explained by the inhomogeneity of the sample thickness. During the preparation of microtome sections the diamond knife can slip on the grains because of their hardness. As a result this technique does not guarantee a constant thickness of the grains from one section to another or even within one section. The maximum damage induced by the irradiations occurs at the penetration depth of the ions. If the sample thickness is smaller than the penetration depth, as it is the case in the grid E2 (Fig. 1), there will be less damage in the irradiated zone. If the sample is thicker than the ions penetration depth (for example grid E1), there could be a non-irradiated zone or a less damaged zone in the deepest part of the sample. In both cases some crystalline or partly crystalline materials may remain in the samples. Consequently, in the spectrum of the irradiated sample, some crystalline IR spectral features will be present and superimposed on the amorphized material spectral signature.

However, if the thickness of the target matches the penetration depth of the incident ions and/or if the irradiation fluence is sufficient, all the crystalline structure disappears and the spectra exhibit two broad and structureless bands corresponding to the stretching vibration of Si-O bonds and to the bending vibration of the O-Si-O bonds. The position of the bending band coincides with the position of the strongest crystalline peak for diopside and enstatite. It seems blue-shifted for olivine but the uncertainty on the peak position is large. The band shape of the amorphized samples is similar to the shape of the structureless band on which the crystalline sub-peak are superimposed in the spectra, if such a decomposition of the crystalline samples spectra can be made (see Figs. 6 and 8). For the three minerals, the stretching mode of the irradiated materials is narrower than the crystalline band and its position seems blue-shifted since the narrow crystalline peaks in the red wing of this band disappear completely (Figs. 6, 8 and 12).

Although the thickness of the different samples does not coincide exactly with the penetration depth of the ions in each sample, it was possible to find areas completely amorphized. This indicates that the amorphization fluence at these energies, for these ions and for these targets are smaller than 10^{18} ions/cm^2, the experimental fluence. This value is only an upper limit and the real fluence may be lower as shown by Jäger et al. (2003) who find an amorphization fluence for enstatite with 50 keV He^+ ions of 9×10^{16} ions/cm^2. However this fluence is larger than for the amorphization of olivine with 4 keV He^+ ions which is in the range of 10^{16}–5×10^{16} ions/cm^2 (Carrez et al. 2002).

All these experimental results show that, for a given ion, the amorphization fluence increases as the ion energy increases. The interaction between the target atoms and the incident ions consists of collisions with the nucleus and with the electronic cloud of the target atoms. Although electronic collisions may displace atoms in the target by electrostatic repulsion, nuclear collisions are the most efficient at displacing atoms and thus causing the amorphization of the target. In general, nuclear collisions contribute most to the energy loss of the incident ions into the target at low energy. The ratio of the energy loss (per Angstrom per incident ion) by ionization with respect to the energy loss by nuclear collisions has been simulated using the program TRIM (Ziegler et al. 1996). It decreases with decreasing energies from ~10–15 for 50 keV He^+ to ~2–4 for 20 keV He^+. At 10 and 4 keV, the energies used by Demyk et al. (2001), the ratio is ~1 and 0.2, respectively. Consequently, the amorphization fluence is lower for low energies, as found experimentally.

The method adopted in this study for the analysis of the samples, infrared spectroscopy, does not allow us to investigate the possible chemical alteration induced by the irradiation of a sample. This is because the spectroscopic changes due to the modifications of the sample structure dominate. However it is, in principle, possible to look for compositional differences between samples irradiated with different ions and/or energies. In practice this is difficult basically because infrared spectroscopy is less sensitive to chemical changes than it is to structural changes. This is particularly true for amorphous materials which have broad and structureless bands which are thus not strongly modified by chemical changes. Comparison of the spectra of enstatite irradiated with 20 and 50 keV He^+ ions does not show any significant differences. In both cases the position of the stretching mode is 9.85 μm. Furthermore differences in the bending mode are not reliable because of the uncertainty in the continuum subtraction. Similarly there is no significant difference between the spectra of olivine irradiated with 20 and 50 keV He^+ ions. The spectra measured at Brookhaven present too much structure for the comparison. From the spectra measured at LURE it is also difficult to conclude since the position of the stretching mode varies from one zone to another among the same sample. From the diopside data we could compare chemical variations induced by different type of ions,

H^+ and He^+. However, as in the case of enstatite and olivine it is difficult to reach any definite conclusions.

5. Astrophysical implications

The results of our previous experiments (Demyk et al. 2001; Carrez et al. 2002) showed that the irradiation of crystalline olivine with 4 to 10 keV He^+ ions efficiently alters the nature of crystalline dust. We found that the long-range structure is destroyed and that the composition of olivine altered through the loss of Mg and O. The present study shows that in addition to olivine, enstatite and diopside, i.e. all the crystalline silicates identified around evolved stars up to now, are amorphized by irradiation with 10 keV H^+ and 20–50 keV He^+. Furthermore, as in the case of olivine irradiated with 4 and 10 keV He^+, we find that irradiation with 10–50 keV H^+ and He^+ induces a change in the compactness of the silicates: the irradiated silicates are porous and contain bubbles of the incident ions implanted into the silicates (Fig. 3).

The experimental conditions that we have considered, are compatible with the physical conditions expected in shocked regions of the diffuse ISM. Indeed, during the propagation of shock waves which ionize and accelerate the ambient gas, energies and fluences compatible with those used in our experiments are reached. Although interstellar silicate grains may be covered with various molecular mantles, ices or complex hydrocarbons, our experiments remain valid for the two following reasons. First, as well established by Whittet et al. (1988), later confirmed by Murakawa et al. (2000), H_2O ice band at 3.3 μm shows an observational threshold in visual extinction (A_v) of about 3. Under this threshold, no ice mantles are detected as a probable result of UV photodesorption of volatile molecules in the diffuse ISM environment. Second, although solid complex hydrocarbons are observed in the diffuse medium (Pendleton et al. 1994; Pendleton & Allamandola 2002), arguably covering the silicate cores, their presence will not protect the underlying silicate structure. Indeed, the stopping power for the fast ions is roughly proportional to Z, the atomic number of the considered element (here C or Si). Thus, only a small fraction of the incident ion energy will be lost in the hydrocarbon layer before entering the silicate core although the precise energy loss is difficult to ascertain owing to uncertainties in the grain models in which the hydrocarbon layer thickness is not precisely known. Further studies, beyond the scope of this paper, are required to account more precisely for this effect.

Jones et al. (1996) have modeled the propagation of shock waves with various velocities in clouds with different densities. For example, they estimate that, in a 100 km s^{-1} velocity-shock, the grains which are not destroyed via sputtering (~65% in mass) are subjected to an irradiation by the accelerated gas with fluences of the order of 10^{16}, 10^{18} (H, H^+)/cm^2 and 10^{15}, 10^{17} (He, He^+)/cm^2 for 5 and 250 nm radius-grain, respectively. These fluences, which do not change dramatically with the shock velocity, are compatible with the amorphization fluence determined in these experiments. Thus, the crystalline silicates present in the ISM would be efficiently amorphized by the passage of a single fast supernovae shock wave.

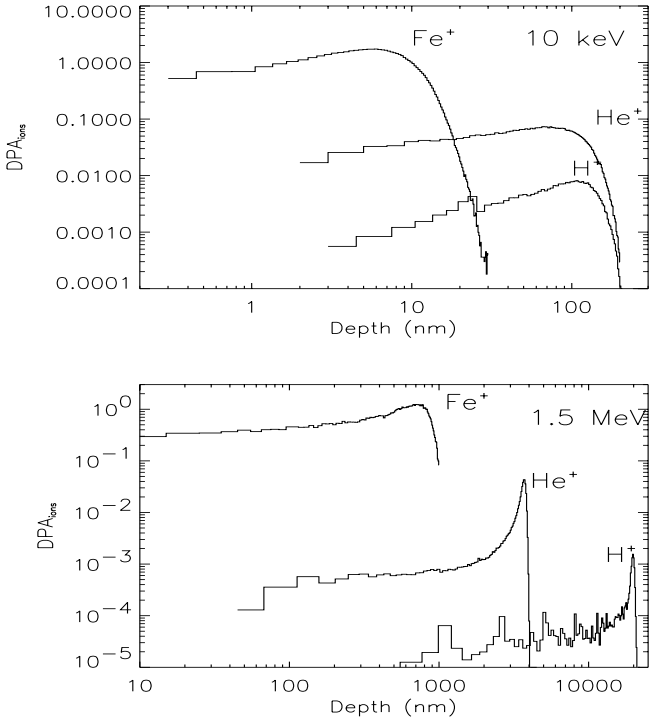

Fig. 13. TRIM simulation of the number of displaced atoms per incident ion per Angstrom for H^+, He^+ and Fe^+ at 10 keV and 1.5 MeV into a forsterite target.

Experiments performed by Day (1977) and Jäger et al. (2003) show that high energy light ions, such as 1 MeV and 400 keV He^+ ions, do not efficiently amorphize silicates. At these energies, light ions interact with the matter mainly via electronic collisions. Since there is very few implantation of the incident ions into the target and limited nuclear collisions these ions are not very efficient at amorphizing grain materials (see Sect. 4). This is illustrated in Fig. 13 which shows the number of displaced atoms (per incident ion/Å) for different ions and energies. Since the amorphization fluence is inversely proportional to the number of displaced atoms, it is clear that the amorphization fluence increases for protons and He^+ ions at high energy compare to low energy. On the other hand, as shown in Fig. 13, high energy heavy ions are more efficient at amorphizing silicates than lighter ions (their amorphization fluence is lower). This is due to the fact that nuclear collisions dominate the interaction with matter at larger energy than for light ions. Heavy ions may thus play a role in the amorphization of silicate grains in the ISM although their abundance is orders of magnitude lower than the abundance of H^+ or He^+ ions.

Ions with low energy and a penetration depth of the order of the grain size may induce chemical changes via selective sputtering. The chemical modifications induced by irradiation have been studied in detail by X-ray Energy Dispersion Spectroscopy and X-ray photoelectron spectroscopy in previous experiments of irradiation of olivine with 4, 10 and 50 keV He^+ (Carrez et al. 2002). It was found that the irradiation induces a loss of oxygen and magnesium in the olivine samples when the ion energy is 4 or 10 keV but no

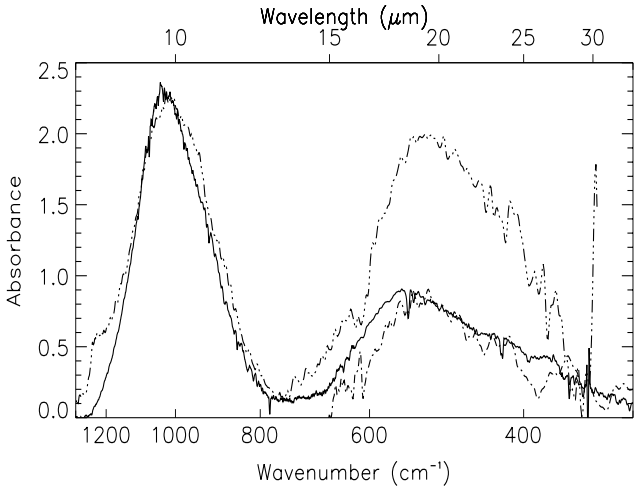

Fig. 14. ISO-SWS spectrum of GC-IRS3 (solid line) compared to the spectra of amorphized entastite (dotted-dashed lines). The laboratory spectra have been scaled to the observed 9.7 μm band (8–30 μm spectrum) and to the observed 18 μm band (15–50 μm spectrum).

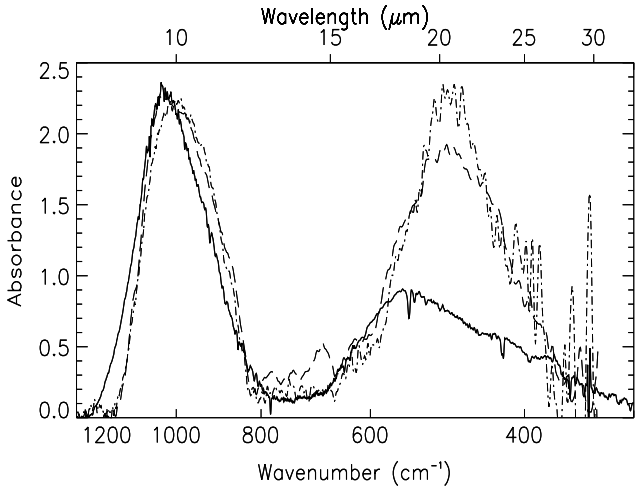

Fig. 15. ISO-SWS spectrum of GC-IRS3 (solid line) compared to the spectrum of amorphized diopside (dotted-dashed lines). The laboratory spectra have been scaled to the observed 9.7 μm band.

chemical change was observed at 50 keV. This is explained by the fact that these changes are due to selective sputtering from the target and are thus expected to be less and less important as the ion energy increases because nuclear collisions diminish. Furthermore, the sputtering yield also decreases because the displacements of the atoms occur at the penetration depth of the ions i.e. far from the surface at 50 keV. A deficiency in magnesium was also observed by Bradley (1994) in olivine irradiated with 20 keV H^+. Dukes et al. (1999) observed the reduction of Si and Fe in olivine irradiated with 1 keV H^+ and 4 keV He^+ ions. No detailed study exists on the chemical alteration of enstatite and diopside. Furthermore, the method adopted in this study for the sample analysis, infrared spectroscopy, does not allow us to investigate chemical changes. Jäger et al. (2003) analyzed the composition of enstatite irradiated with 50 keV He^+ and did not observe any chemical change, which is not surprising considering results of Carrez et al. (2002) on olivine. Although it is difficult to estimate the importance of this phenomenon in the ISM, these results show that grains having a size comparable to the implantation depth of the ions may undergo an important chemical fractionation via the selective sputtering of their atoms. More experiments are needed on enstatite and diopside irradiated with low energy ions ($\leq$10 keV ions) and also on olivine, using other ions than He^+.

In the diffuse ISM all the silicates may be submitted to some irradiation and the spectra of amorphized olivine, enstatite and diopside may thus contribute to the ISM spectra. However, since the amount of crystalline silicate injected into the ISM per unit volume and unit time is poorly known, it is difficult to estimate the expected contribution of this irradiated population to the observed spectra of the ISM. A qualitative comparison of the IR spectra of the amorphized silicates with the SWS spectrum of the Galactic Center GC IRS3 is presented Figs. 14–16. The ISO spectrum has been divided by an arbitrary continuum. This procedure is not as rigorous as a full radiative transfer calculation, in particular, the ratio of the stretching to bending mode is not well constrained. The line of sight toward the Galactic Center contains both dense and diffuse clouds. However, the low optical depth of the ice species in GC IRS3 (Chiar et al. 2000) shows that the dust is mainly coming from diffuse clouds. Furthermore, the absorbance in GC IRS3 is very similar to the average silicate feature derived by Dudley & Wynn-Williams (1997) from the modeling of the ISO-SWS spectra of the three Wolf-Rayet stars WR98a, WR112 and WR118 (see the thin line in Fig. 5 of their article). Since lines of sight toward Wolf-Rayet stars are representative of the diffuse ISM and are thought to contain a minor contribution from molecular clouds, we can consider that the silicate feature derived from the spectrum of GC IRS3 is characteristic of diffuse clouds.

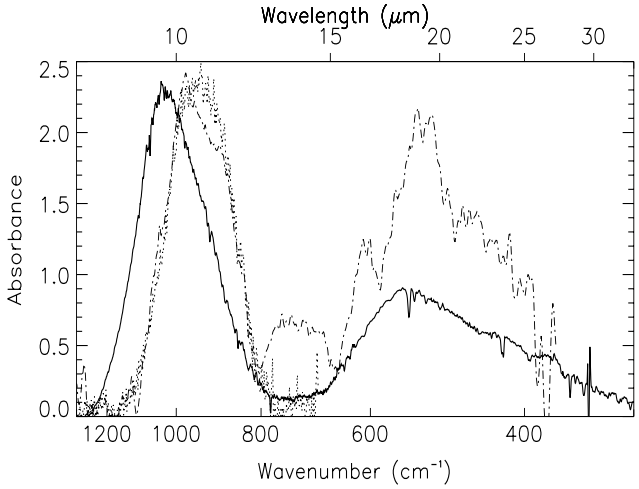

Fig. 16. ISO-SWS spectrum of GC-IRS3 (solid line) compared to the spectra of amorphized olivine (dashed line: data from the NSL, dotted line: data from the LURE). The laboratory spectra have been scaled to the observed 9.7 μm band.

The spectra of amorphized diopside and olivine do not fit the observed spectrum very well. The position of the silicate bands is redshifted compare to the observations. The stretching mode is at $\lambda_{peak} \sim 10\,\mu$m and 10.3–10.6 μm for irradiated diopside and olivine respectively (see Sects. 3.2 and 3.3), whereas it peaks at ~9.7 μm in the spectrum of GC IRS3. Similarily, the bending mode of the silicate is at ~18.3 μm in the spectrum of GC IRS3 and at ~24.45 μm in the spectrum of irradiated diopside. The bending mode of irradiated olivine contains too much structure to be compare with the observations. These spectra of irradiated olivine and diopside may nevertheless contribute to the overall spectra of the ISM if their abundance is not too high.

Although the silicate bands in the spectrum of the irradiated enstatite spectra are slightly red shifted compare to the observations ($\lambda_{peak} \sim 9.85$ and ~18.8 μm for the irradiated entatite compare to ~9.7 μm and 18.3 μm in GC IRS3), the amorphized enstatite spectrum fits rather well the GC IRS3 spectrum. The ratio of the stretching to the bending mode is not well reproduced. However this problem arises in all the attempts to fit the ISM silicate bands (e.g. Mathis 1998). It may come from the analog used for the fit or from the continuum subtraction at long wavelengths. In our case, it can also arise from the continuum subtraction in the experimental spectrum. The good agreement between the observations and the irradiated enstatite spectrum is surprising since the ISM silicate bands are usually fitted with glassy olivine (Mathis 1998). This illustrates the difficulty in assigning these bands and in constraining the composition of the amorphous silicate component. Amorphous materials may have different microscopic structures, for example glassy silicates (e.g. Dorschner et al. 1995) which have a short-range order compared to amorphous silicates produced in smokes (e.g. Hallenbeck et al. 2000). This results in differences in the infrared spectroscopic characteristics of the silicates. The samples analyzed in this study are made from a crystalline lattice in which a multitude of defects are created until nothing or almost nothing remains from the original atomic arrangement. The resulting structure is chaotic and contains some degree of porosity in the form of bubbles, empty or filled with implanted ions (Demyk et al. 2001). These bubbles are easily seen in Fig. 3c. These irradiated samples are thus very different from glassy silicates having the same composition (Dorschner et al. 1995) and this probably explains the spectral differences between them. However, concerning the assignment of the interstellar bands and the study of the composition of the interstellar silicates, this diversity in the spectral signatures of amorphous silicates analogs is puzzling and emphasizes the equivocal nature of proposed identifications.

6. Conclusion

We have studied the structural changes of crystalline silicates, forsterite, diopside and enstatite, induced by irradiations with 20 and 50 keV He^+ and 10 keV H^+ with fluences of 10^{18} ions/cm^2. We observe that every sample is amorphized for all the energies and incident ions considered. This gives an upper limit to the amorphization fluence of 10^{18} ions/cm^2. In addition we observe that implanted ions form bubbles in the minerals, modifying their porosity. The IR signature is strongly modified by the irradiation. The sharp and narrow peaks characteristic of the crystalline structure before irradiation completely disappear after irradiation. The resulting spectra present two broad and structureless bands at ~9.7–10.3 and 17–18 μm, corresponding to the stretching and bending mode of the Si-O and O-Si-O bands in the silicates, and are characteristic of an amorphous material. Comparison with ISO-SWS observations of the Galactic Center shows that the interstellar spectrum is better reproduced with irradiated enstatite than with irradiated olivine or diopside. Even though the main component responsible for the interstellar silicate bands is the amorphous silicates formed around evolved stars, the spectral characteristics of these three irradiated silicates may contribute to the interstellar bands.

TRIM simulations show that low energy light ions and high energy heavy ions are the most efficient at amorphizing silicates. High energy light ions will not significantly alter silicates and low energy heavy ions will induce damage only in a very thin layer of the grains. Since in the ISM heavy ions are several orders of magnitude less abundant than light ions such as H^+ and He^+, and since the experimental conditions used in this study are compatible with the interstellar case we conclude that H^+ and He^+ ions with energies lower than 50 keV are the most favorable for efficiently modifying the interstellar silicate structure. Ions with such energies may be found in the diffuse ISM in regions where high velocity supernovae shock waves propagate.

Acknowledgements. We would like to thank Nicolas Chauvin and D. Le Du for having performed the irradiation experiments at the CSNSM in Orsay. We are very grateful to Paul Dumas from the LURE for his help with IR microspectroscopy and to Larry Carr and Gregory Smith for their very skillful help for the micro-spectroscopic measurements at the NLS, Brookhaven. We would like to thank the referee, J. Bowey, for her comments that have greatly helped to improve this paper. Support from the PNP-CNRS and PCMI-CNRS is acknowledged.

References

Borg, J., Chaumont, J., Langevin, Y., et al. 1979, in The ancient sun: Fossil record in the earth, moon and meteorites, Boulder, CO, October 16–19, 431
Borg, J. 1982, Thèse, Université de Paris-Sud
Bradley, J. P. 1994, Science, 265, 925
Carrez, Ph., Leroux, H., Cordier, P., et al. 2001, Philos. Mag., A81, 2823
Carrez, Ph., Demyk, K., Cordier, P., et al. 2002, M&PS, 37, 1599
Chiar, J. E., Tielens, A. G. G. M., Whittet, D. C. B., et al. 2000, A&A, 537, 749
Day, K. L. 1977, MNRAS, 178, 49
Demyk, K., Jones, A. P., Dartois, E., et al. 1999, A&A, 349, 267
Demyk, K., Dartois, E., Wiesemeyer, H., et al. 2000, A&A, 364, 170
Demyk, K., Carrez, Ph., Leroux, H., et al. 2001, A&A, 368, L38
Dorschner, J., Begemmann, B., Henning, T., et al. 1995, A&A, 300, 503

Dudley, C. C., & Wynn-Williams, C. G. 1997, ApJ, 488, 720
Dukes, C. A., Baragiola, R. A., & McFadden, L. A. 1999, JGR, 104, 1865
de Graauw, T., Haser, L. N., Beintema, D. A., et al. 1996, A&A, 315, L49
Hallenbeck, S. L., Nuth, J. A. III, & Nelson, R. N. 2000, ApJ, 535, 247
Jäger, C., Fabian, D., Schrempel, F., et al. 2003, A&A, 401, 57
Kemper, F., de Koter, A., Waters, L. B. F. M., Bouwman, J., & Tielens, A. G. G. M. 2002, A&A, 384, 585
Li, A., & Draine, B. 2001, ApJ, 550, L213
Lutz, D., Feuchtgruber, H., Genzel, R., et al. 1996, A&A, 315, L269
Mathis, J. S. 1998, ApJ, 497, 824
Murakawa, K., Tamura, M., & Nagata, T. 2000, ApJS, 128, 603
Pendleton, Y. J., Sandford, S. A., Allamandola, L. J., et al. 1994, ApJ, 437, 683
Pendleton, Y. J., & Allamandola, L. J. 2002, ApJS, 138, 75
Schutte, W. A., van der Hucht, K. A., Whittet, D. C. B., et al. 1998, A&A, 337, 261
Sylvester, R. J., Kemper, F., Barlow, M. J., et al. 1999, A&A, 352, 587
Waelkens, C., Waters, L. B. F. M., de Graauw, M. S., et al. 1996, A&A, 315, L245
Waters, L. B. F. M., Molster, F. J., de Jong, T., et al. 1998, A&A, 315, L361
Whittet, D. C. B., Bode, M. F., Longmore, A. J., et al. 1988, MNRAS, 233, 321
Ziegler, J. F., Biersack, J. P., & Littmark, U. 1996, The Stopping and Range of Ions in Solids (USA, New York: Pergamon Press)